Generation and Characterization of Ionic and Neutral $P(OH)_2^{+/\cdot}$ in the Gas Phase by Tandem Mass Spectrometry and Computational Chemistry

R. Srikanth and R. Srinivas
National Center for Mass Spectrometry, Indian Institute of Chemical Technology, Hyderabad, India

K. Bhanuprakash
Inorganic Chemistry Division, Indian Institute of Chemical Technology, Hyderabad, India

S. Vivekananda, E. A. Syrstad, and F. Tureček
Department of Chemistry, University of Washington, Seattle, Washington, USA

The bicoordinated dihydroxyphosphenium ion $P(OH)_2^+$ ($\mathbf{1}^+$) was generated specifically by charge-exchange dissociative ionization of triethylphosphite and its connectivity was confirmed by collision induced dissociation and neutralization-reionization mass spectra. The major dissociation of $\mathbf{1}^+$ forming PO^+ ions at *m/z* 47 involved another isomer, O=P—OH_2^+ ($\mathbf{2}^+$), for which the optimized geometry showed a long P—OH_2 bond. Dissociative 70-eV electron ionization of diethyl phosphite produced mostly $\mathbf{1}^+$ together with a less stable isomer, $HP(O)OH^+$ ($\mathbf{3}^+$). Ion $\mathbf{2}^+$ is possibly co-formed with $\mathbf{1}^+$ upon dissociative 70-eV electron ionization of methylphosphonic acid. Neutralization-reionization of $\mathbf{1}^+$ confirmed that $P(OH)_2^{\cdot}$ (**1**) was a stable species. Dissociations of neutral **1**, as identified by variable-time measurements, involved rate-determining isomerization to **2** followed by fast loss of water. A competitive loss of H occurs from long-lived excited states of **1** produced by vertical electron transfer. The *A* and *B* states undergo rate-determining internal conversion to vibrationally highly excited ground state that loses an H atom via two competing mechanisms. The first of these is the direct cleavage of one of the O—H bonds in **1**. The other is an isomerization to **3** followed by cleavage of the P—H bond to form O=P—OH as a stable product. The relative, dissociation, and transition state energies for the ions and neutrals were studied by ab initio and density functional theory calculations up to the QCISD(T)/6–311+G(3df,2p) and CCSD(T)/aug-cc-pVTZ levels of theory. RRKM calculations were performed to investigate unimolecular dissociation kinetics of **1**. Excited state geometries and energies were investigated by a combination of configuration interaction singles and time-dependent density functional theory calculations. (J Am Soc Mass Spectrom 2002, 13, 250–264) © 2002 American Society for Mass Spectrometry

Over the years a great deal of attention has been focused on the chemistry of phosphorus oxoacids, some of which belong to the family of low coordinated phosphorus compounds. Phosphorus oxoacids are believed to play an important role in the chemistry and biochemistry of phosphorus containing compounds and have been extensively studied by experiment and theory [1–5]. Low coordinated dithiophosphanes are also known to be reactive intermediates and some of them have been isolated as stable ligands in complexes [6, 7]. Unfortunately, direct evidence for the existence of these species as stable monomeric entities is scarce due to facile intermolecular reactions. The neutralization- reionization mass spectrometry (NRMS) technique [8–13] has been established as a powerful tool for investigating the stabilities and structures of highly reactive and elusive transient species in the rarefied gas phase and it has been successfully used to generate and characterize some of the low coordinated phosphorus species. Keck and Terlouw and their co-workers have provided NRMS experimental evidence for the gas phase existence of (methylthio) thioxophosphane (CH_3S-P=S) [14], phosphenethiol (H_2P-SH) [15], phosphenedithiol HP $(SH)_2$ [16],

Published online January 16, 2002

Address reprint requests to Dr. F. Tureček, Department of Chemistry, University of Washington, Bagley Hall, Box 351700, Seattle, WA 98195-1700, USA. E-mail: turecek@chem.washington.edu

This article is registered as IICT Communication No. 4817.

1044-0305/02/$20.00
PII S1044-0305(01)00360-9

Received August 30, 2001
Revised November 16, 2001
Accepted November 16, 2001

thioxophosphane HPS and its tautomer HSP [17] molecules. Gu and Tureček [18] have reported an NRMS study on several oxygenated phosphorus species, e.g., PO, CH_3OPH, CH_3OPOH, CH_3OPOCH_3, and $(CH_3O)_2PO$. Vivekananda, Srinivas, and coworkers recently reported [19, 20] on the generation and characterization of low coordinated phosphorus species, viz., CH_3O-P=O, CH_3S-P=O and NH_3PO by using a combination of tandem mass spectrometric techniques. Tureček et al. [21] also have demonstrated the importance of Franck-Condon effects in the dissociations and isomerizations of gas-phase phosphorus oxoacids and radicals, mainly $P(OH)_3$ and $P(OH)_4^{\cdot}$ and their corresponding isomeric species. This NRMS study revealed that vertical neutralization of stable $P(OH)_4^+$ produced vibrationally excited unstable $P(OH)_4^{\cdot}$ whereas the tricoordinated $P(OH)_3^{+\cdot/o}$ and its isomer $HPO(OH)_2^{+\cdot/o}$ formed stable molecules on the ms time scale of NRMS experiments. In contrast to these tri and tetra coordinated hydroxyphosphoranyl species that were treated extensively by theory [22–28], bicoordinated phosphoranyl radicals, e.g., $P(OH)_2^{+\cdot}$, received much less attention [29–31]. Although Tureček et al. [21] briefly mentioned this species as one of the dissociation products of trihydroxyphosphane, no detailed study of this radical or its isomers has been reported. We therefore decided to investigate $P(OH)_2^{+\cdot}$ by a combination of tandem mass spectrometric experiments and theoretical calculations.

Experimental

The mass spectrometric experiments in Hyderabad were carried out using a VG Micromass Autospec M mass spectrometer of E_1BE_2 geometry [19] (E denotes an electric sector and B, magnetic sector). The instrument has two collision chambers (Cls-2 and Cls-3) and an intermediate deflector electrode, all in the third field free region (between E_1B and E_2).

Methylphosphonic acid (**I**) diethyl phosphite (**II**) and triethyl phosphite (**III**) were commercially available (Aldrich, Milwaukee, WI) and were used without further purification. Di-([$^2H_5$]ethyl)phosphite (**IIa**) was synthesized from PCl_3 and [$^2H_6$]ethanol (both Aldrich) according to a literature procedure [32]. **I** was introduced into the ion source via the direct insertion probe and **II** and **III** through the liquid inlet system under the following conditions: source temperature, 250 °C; electron energy, 70 eV; trap current, 250 μA.; acceleration potential, 7 kV. Accurate mass measurements of the ion at *m/z* 65 from **I–III** were obtained at a resolution of $m/\Delta m$=7000 (10 % valley definition), using the data system. Kinetic energy release values (eV) in metastable-ion dissociations forming *m/z* 47 from precursors I–III were measured from peak widths at half maximum and corrected for the main beam peak width [33, 34]. The collision induced dissociation mass spectra (CID) were recorded by mass selecting the beam of *m/z* 65 ions using E_1B (MS-1), with 7 keV translational energy and allowing collisions with oxygen in the collision cell Cls-3; the resulting ions were analyzed by scanning E_2 (MS-2). CID mass spectra of *m/z* 65 ions were also recorded in the FFR-1 using the linked scan technique (B/E = constant).

Charge-exchange ionization with $CO_2^{+\cdot}$ to produce *m/z* 65 ions from **III** under CI conditions was performed in a tight CI source at 7×10^{-5} torr of CO_2, as read on the source ion gauge. The NR experiments were conducted by mass selecting the beam of ions of *m/z* 65 with E_1B (MS-1) and neutralizing them in Cls-2 with xenon. The remaining ions were deflected away from the beam of neutrals by means of a deflector electrode (+5 kV). The neutral beam was reionized in Cls-3 with O_2 target gas and the resulting ions were recorded by scanning E_2. The spectra shown are accumulations of 25–50 scans.

The measurements in Seattle were made on a tandem quadrupole acceleration-deceleration mass spectrometer described previously [35]. Electron ionization was used to generate *m/z* 65 ions from **II** and **III** and *m/z* 67 ions from di-([$^2H_5$]ethyl) phosphite in a standard electron ionization source. Typical ionization conditions were as follows: electron energy 70 eV, emission current 500 μA, temperature 200–250 °C. Charge-exchange ionization with CO_2 was performed in a tight chemical ionization source at 2×10^{-4} torr CO_2 as read on the ionization gauge placed at the diffusion pump intake; this corresponds to 0.2–0.3 torr in the ion source. The partial pressure of **III** was 2×10^{-6} torr in these measurements. Stable precursor ions were passed through a quadrupole mass filter operated in the radio-frequency-only mode, accelerated to the total kinetic energy of 8250 eV and neutralized in a differentially pumped collision cell (cell-I) floated at −8170 V. The precursor ion lifetimes were 30–40 μs. For cations and radical cations neutralization is achieved by collisions with dimethyldisulfide (DMDS) that was admitted to cell-I at a pressure such as to achieve 70 % transmittance of the precursor ion beam. The ions and neutrals were allowed to drift to a four segment conduit, where the ions were reflected by the first segment floated at +250 V. The flight times for neutral species in standard NRMS measurements were 3.85 μs. The fast neutral species were reionized in a second collision cell (cell-II) by collision with oxygen at a pressure adjusted such as to achieve 70 % transmittance of the precursor ion beam. The ions formed in cell-II were decelerated, energy filtered, and analyzed by a quadrupole mass filter operated at unit mass resolution. The instrument was tuned daily to maximize the ion current of reionized $CS_2^{\cdot+}$. Typically, 40 repetitive scans were accumulated per spectrum. Collisional activation of neutral intermediates (NCR) was performed by admitting helium into the neutral-drift region at pressures allowing 70 % precursor ion transmittance. Neutral species were generated in cell-I and the remaining ions were reflected (see above). The neutral-drift region was floated at +250 V to reject any ions formed there by collisional

reionization. Neutral dissociation products were allowed to drift to cell-II where they were reionized by collisions with O_2 at pressures allowing 70 % beam transmittance. Variable-time measurements were carried out as described previously [36, 37]. The flight times of neutral species in these measurements were 0.40, 1.12, 1.84, and 2.56 μs.

Calculations

Standard ab initio and density functional theory calculations were performed using the GAMESS UK [38–40] and Gaussian 98 [41] suites of programs. An initial set of geometries was obtained by using Becke's hybrid functional, B3LYP [42–44], and the 6–31G(d,p) basis set. The radical and selected ion geometries were refined by optimizations that used B3LYP and Moller-Plesset perturbational calculations with all electron excitations, MP2(FULL) [45], and the larger 6–311 + G(2d,p) basis set which incorporated diffuse functions and two shells of five d-functions on P and O [46]. Stationary points were characterized by harmonic frequency analysis as local minima (all real frequencies) and first-order saddle points (one imaginary frequency). Spin unrestricted (UB3LYP and UMP2) calculations were used for open-shell systems. Spin contamination in these calculations was low for all local minima and saddle points, as judged from the spin operator expectation values, S^2, which were 0.75–0.76 for UB3LYP and 0.76–0.8 for UMP2. Annihilation of higher spin states [47, 48] was applied to the UMP2 energies that corrected the S^2 values to 0.75 and resulted in projected total energies, PMP2, that were 1.5–2.2 millihartree lower than the UMP2 ones. The B3LYP optimized geometries are reported here; the MP2(FULL) geometries are available from the correspondence author upon request.

Improved energies were obtained by single-point calculations at five levels of theory. These included composite G2(MP2) [49] and G2 [50] schemes that use quadratic configuration interaction [51] calculations with frozen core excitations, QCISD(T) with the 6–311G(d,p) basis set, and basis set expansion up to effective 6–311+G(3df,2p) through MP2 and MP4(SDTQ) single-point calculations. For selected systems, these were compared with QCISD(T)/6–311+G(3df,2p) calculations that used the full large basis set. In addition, coupled cluster [52] single-point calculations with single, double, and perturbational triple excitations, CCSD(T) [53], were carried out with Dunning's correlation-consistent triple-ζ basis set augmented with diffuse functions, aug-cc-pVTZ [54]. Finally, B3LYP and MP2 calculations performed with the 6–311+G(3df,2p) basis set were combined in an empirical procedure, B3-MP2 (B3-PMP2 for spin-projected energies), that has been described previously [55–58].

The calculated transition state energies were used for Rice-Ramsperger-Kassel-Marcus (RRKM) calculations of unimolecular rate constants, k_{uni}, using Hase's program [59] that was recompiled and run under Windows NT [60]. The RRKM calculations used direct count of quantum states in 2 kJ mol^{-1} intervals from the transition state energy up to 360 kJ mol^{-1} excitation. Rotational states were treated adiabatically and the rate constants, $k(E,J,K)$, were Boltzmann-averaged over the population of rotational states at 523 K, which corresponded to the typical ion source temperature in the spectra measurements.

Calculations of excited electronic states were performed as reported previously [56–58]. Gradient optimizations were done with configuration-interaction singles (CIS) [61] and the 6–311+G(2d,p) basis set which also provided harmonic frequencies. Improved excited state energies were obtained by single-point, time-dependent density-functional theory calculations, TD-B3LYP [62], and the 6–311+G(3df,2p) basis set.

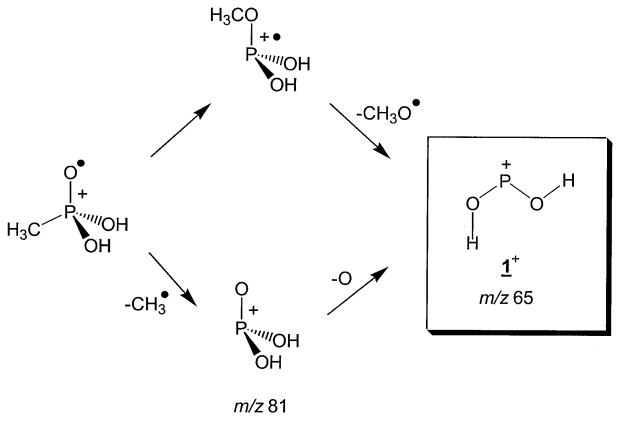

Scheme 1

Results and Discussion

Preparation and Dissociations of $[P,O_2,H_2]^+$ Ions

Oxygenated phosphorus radicals of the $[P,O_2,H_2]$ type are transient species that do not have obvious stable neutral precursors to be used for gas-phase generation. Our approach to $[P,O_2,H_2]$ radicals relied on the generation of stable $[P,O_2,H_2]^+$ cations, which are accessible by dissociative electron ionization of several stable organophosphorus compounds, e.g., methylphosphonic acid (**I**), diethyl phosphite (**II**), and triethyl phosphite (**III**) [63].

The 70 eV electron-ionization spectrum of methylphosphonic acid affords a relatively weak peak at *m/z* 65 (8 %) corresponding to $[P,O_2,H_2,]^+$ ions denoted as ion ***A***. The elemental composition of this ion has been confirmed by high-resolution measurements and isobaric impurities were not detected. The formation of these ions from the methylphosphonic acid cation radical, $[CH_3PO_3H_2]^{+\cdot}$, can be envisaged to proceed by two different pathways, e.g., (1) loss of $CH_3^{\cdot}$ followed by O, and (2) a direct elimination of $OCH_3^{\cdot}$ (Scheme **1**). Evidence for these pathways follows from metastable ion dissociations of $[CH_3PO_3H_2]^{+\cdot}$ and the fragment ion at *m/z* 81. The elimination of $OCH_3^{\cdot}$ requires a rearrange-

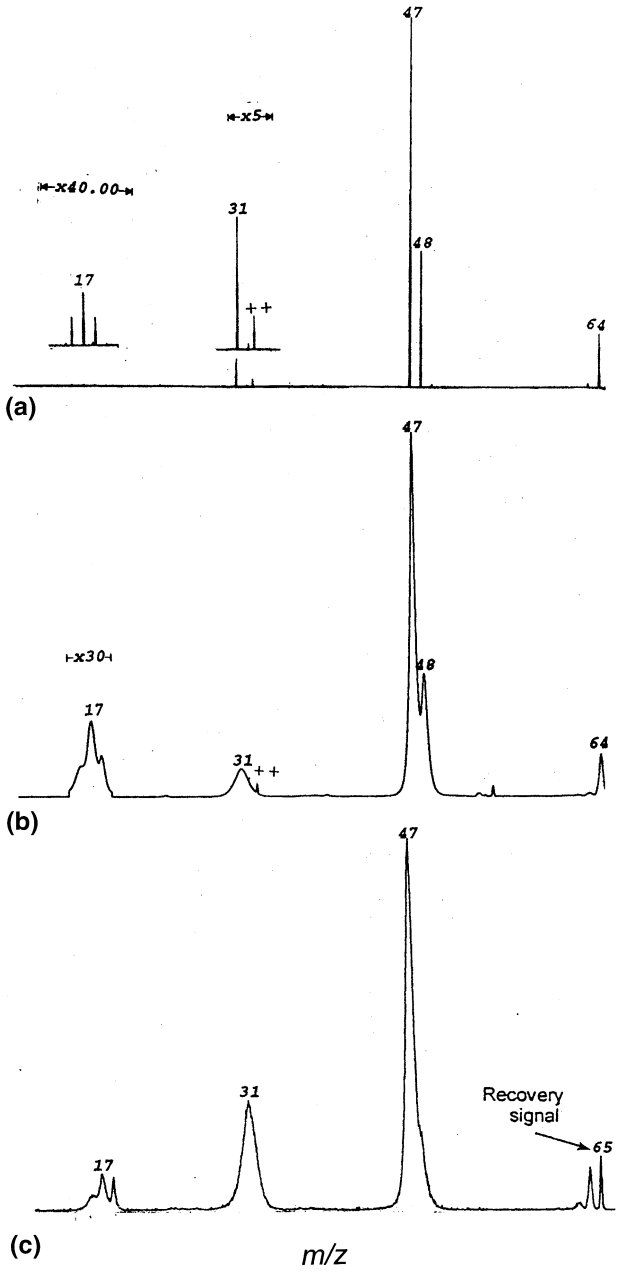

Figure 1. CID spectra (O_2, 70 % T) of ion ***A*** from methylphosphonic acid. (**a**) B/E CID. (**b**) MIKES-CID. (**c**) $^{+}NR^{+}$ (Xe, 70 % T/O_2, 70 % T) mass spectrum.

ment in $[CH_3PO_3H_2]^{+\cdot}$ involving a 1,2-methyl migration to the oxygen prior to dissociation to form $[P,O_2,H_2]^{+}$. Another possible reaction mechanism may involve methyl group and hydrogen migrations in $[CH_3PO_3H_2]^{+\cdot}$ resulting in an elimination of a CH_2OH radical. These mechanisms were not distinguished in the present study.

Ion ***A*** was characterized by metastable-ion (MI) and CID spectra; the latter were recorded as MIKE and B/E scans (Figure 1). Besides obvious differences in mass resolution in these scans, the MIKE and B/E CID spectra sampled precursor ions of different lifetimes.

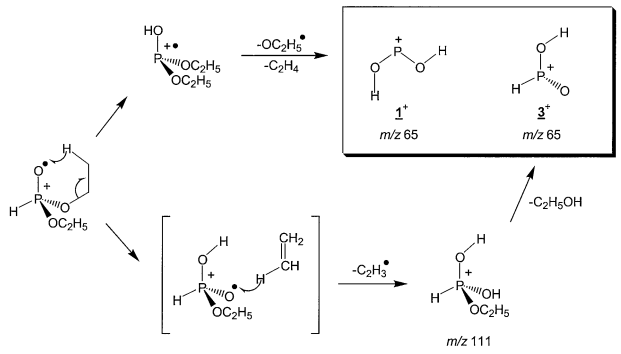

Scheme 2

The metastable-ion spectrum of ***A*** was weak and showed PO^+ at *m/z* 47 (loss of H_2O) as the predominant fragment. This MI peak showed a composite gaussian profile that was characterized by the value of kinetic energy release at half maximum, $T_{0.5}$ = 0.074 V (7 kJ mol^{-1}). The composite shape of the peak was inferred from fitting a gaussian-like peak according to eq 1), where H_0 is the peak height at maximum, w is the peak width at height H, and a = ln 2 [64].

$$H = H_0\exp(-aw^n) \quad (1)$$

which gave n = 1.2 as opposed to n = 2 for a pure Gaussian peak. The presence of a composite MI peak indicates more than one dissociation pathway for the elimination of water, as discussed below.

The CID spectra of ion ***A*** displayed the base peak at *m/z* 47 (PO^+) due to the loss of H_2O. Elimination of water is typical of dissociations of oxygenated phosphorus cations, e.g., $P(OH)_4^+$ and $P(OH)_3^{+\cdot}$ [21]. The other fragments in CID spectra of ***A*** were $[P,O_2,H]^{+\cdot}$ at *m/z* 64 (loss of H), $[POH]^{+\cdot}$ at *m/z* 48 (loss of OH), P^+ at *m/z* 31, and the weakly intense peaks of $H_2O^{+\cdot}$, OH^+, and $O^{+\cdot}$ at *m/z* 18-16. The CID of ion ***A*** were compatible with bond connectivities in HO—P—OH^+ (**1**$^+$) and O—P—OH_2^+ (**2**$^+$) for the *m/z* 65 ions. The ion structures and energies are discussed later in the paper.

The 70 eV electron ionization of diethyl phosphite yields abundant (80 %) *m/z* 65 ions $[P,O_2,H_2]^+$ (denoted as ion ***B***) whose elemental composition was confirmed by high resolution measurements. Loss of a vinyl radical followed by an ethanol molecule from the molecular ion can account for the formation of ion ***B*** (Scheme **2**). This fragmentation pathway has been confirmed from the MI spectra of the molecular ion and the $(M - C_2H_3)^+$ ion at *m/z* 111. The MI spectrum of ion ***B*** showed a dominant peak of PO^+ that had a composite gaussian shape, which was characterized by $T_{0.5}$ = 0.084 eV (8 kJ mol^{-1}) and n = 1.38. The CID (both B/E and MIKE scans) spectra of ion ***B*** (Figure 2) showed all the fragment ions that were present in the CID spectra of ion ***A***, but with somewhat different relative abundances. The main differences in the CID spectra were as follows: The spectrum of ion ***B*** showed (1) a more

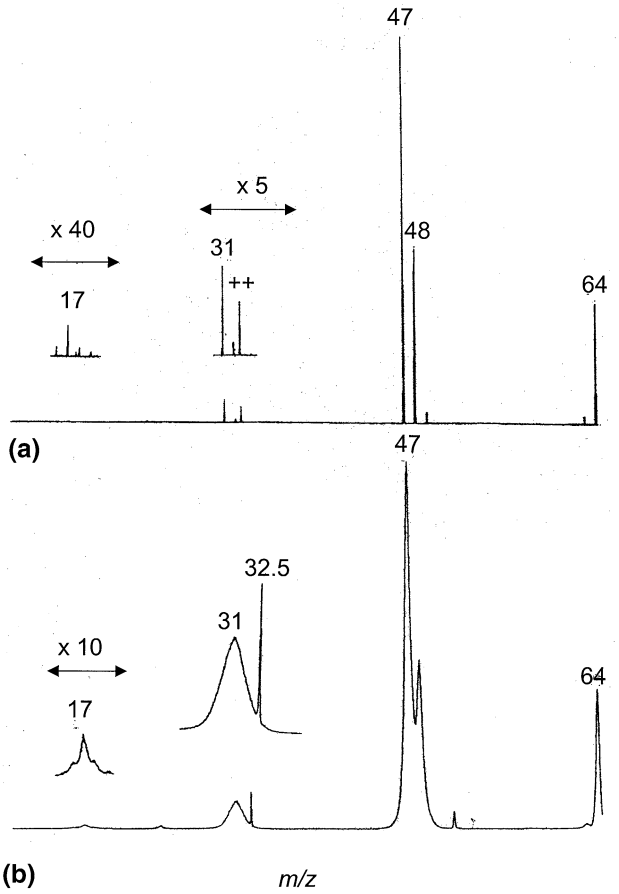

Figure 2. CID spectra (O_2, 70 % T) of ion ***B*** from diethyl phosphite. (**a**) B/E CID. (**b**) MIKES-CID.

abundant fragment at *m/z* 64 due to loss of H, (2) a higher $[HPO]^+/[PO]^+$ abundance ratio, 0.45 compared to 0.34 for ***A***, and (3) a more abundant doubly charged $[P,O_2,H_2]^{+2}$ ion at *m/z* 32.5. The B/E CID spectrum of ***B*** also shows more abundant PH^+ peak at *m/z* 32 and a lower $[H_2O]^+/[OH]^+$ ratio than from ***A***. The higher proportion of PH^+ and HPO^+ formation in CID of ***B*** may indicate the presence of yet another ion structure, H—P(O)OH^+ ($\mathbf{3}^+$), which is also compatible with the presence of a H—P bond in the diethyl phosphite precursor. However, the MIKE and CID spectra alone do not rule out the presence of isomeric structures $\mathbf{1}^+$ and $\mathbf{2}^+$ in ***B***.

A $[P,O_2,H_2]^+$ ion (***C***) is formed abundantly (85 %) [63] from triethyl phosphite by elimination of ethoxyl radical (*m/z* 121) followed by two ethylene molecules and/or by elimination of a vinyl radical (*m/z* 139)

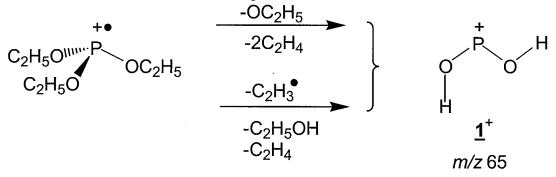

Scheme 3

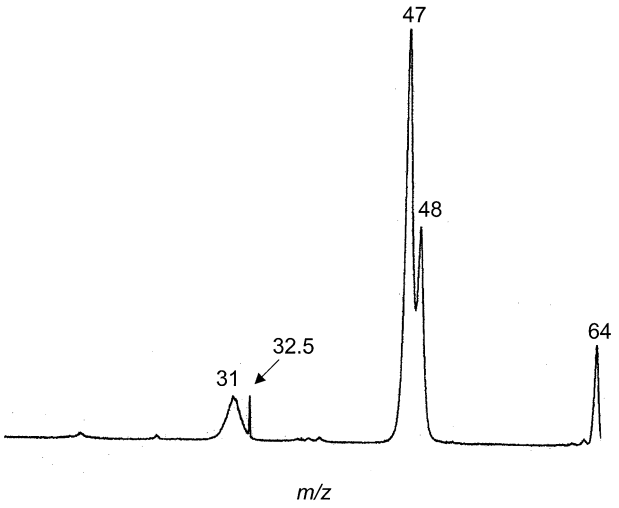

Figure 3. CID spectrum of ion ***C*** from CE ionization of triethyl phosphite.

followed by ethanol, and ethylene. Scheme **3** shows the formation of ion ***C*** with structure $\mathbf{1}^+$, as discussed below. Ion ***C*** showed characteristics that were intermediate between those of ***A*** and ***B***. In particular, the MI-spectrum showed a dominant peak of PO^+ of $T_{0.5}$ = 0.096 eV (9 kJ mol^{-1}) and n = 1.14, and the CID spectrum displayed the fragments at *m/z* 64 (similar to ***A***), 48 (similar to ***B***), and 32.5 (similar to ***A***) (Figure 3).

Since 70-eV electron ionization imparts a broad range of energies in the ions formed and since the lowest dissociation energies in ions $\mathbf{1}^+$–$\mathbf{3}^+$ are 90–204 kJ mol^{-1} (vide infra), the non-dissociating ions that are probed by CID and NR can have substantial internal energies that may affect dissociation or isomerization. In order to prepare ions with a narrower range of internal energies, we used charge-exchange ionization (CE) with CO_2 (IE = 13.78 eV) [63]. The choice of the charge-exchange reagent gas was guided by G2 calculations that provided the enthalpy of formation for $\mathbf{1}^+$, $\Delta H_{f,298}$ = 394 kJ mol^{-1}. When combined with the enthalpies of formation of triethyl phosphite (−813.4 kJ mol^{-1}) [65], $C_2H_5O^{\cdot}$ (−18 kJ mol^{-1}),* and ethylene (52.5 kJ mol^{-1}) [63], the appearance energy of $\mathbf{1}^+$ is calculated as $AE(\mathbf{1}^+)$ = 13.4 eV. Charge-exchange ionization of triethyl phosphite with $CO_2^{+\cdot}$ therefore imparts a total of 13.8–13.4 = 0.4 eV excess energy to drive the dissociation, and this excess is distributed among the neutral products and $\mathbf{1}^+$, forming the ion with low internal energy. The alternative dissociation pathway by elimination of $C_2H_3^{\cdot}$, C_2H_5OH, and C_2H_4 of enthalpies of formation 295,† −235.3 [63], and 52.5 kJ mol^{-1}, respectively, requires $AE(\mathbf{1}^+)$ = 13.7 eV. In addi-

* From the enthalpy of formation of $C_2H_5O^-$ (−183 to −186 kJ mol^{-1}) [66, 67] and the electron affinity of $C_2H_5O^{\cdot}$ (1.712 eV) [68].

† The enthalpy of formation of the vinyl radical has been in dispute. From the tabulated proton affinity of $C_2H_3^{\cdot}$ (755 kJ mol^{-1}) [63], one derives $\Delta H_{f,298}(C_2H_3^{\cdot})$ = 292 kJ mol^{-1}, whereas the C—H bond-dissociation energy (138 ± 2 kJ mol^{-1}) [69] gives $\Delta H_{f,298}(C_2H_3^{\cdot})$ = 307 kJ mol^{-1}. The CCSD(T)/aug-cc-pVTZ dissociation energy of the C—H bond in ethylene, D(C—H) = 460 kJ mol^{-1}, gives $\Delta H_{f,298}(C_2H_3^{\cdot})$ = 295 kJ mol^{-1} which is the value used here for the appearance energy estimate.

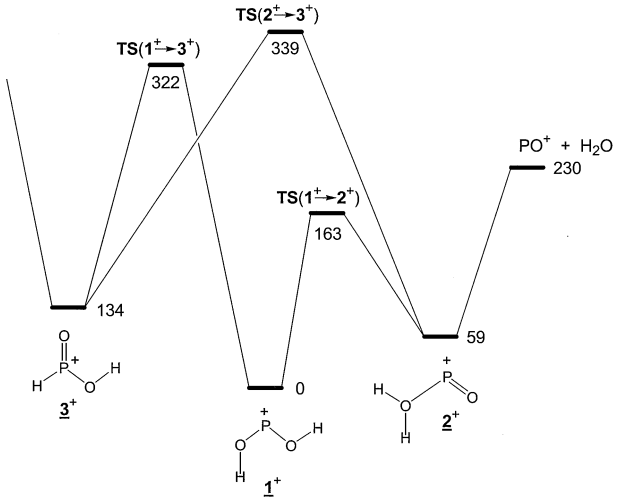

Figure 4. B3LYP/6–31G(d,p) potential energy surface for $\mathbf{1}^+$–$\mathbf{3}^+$.

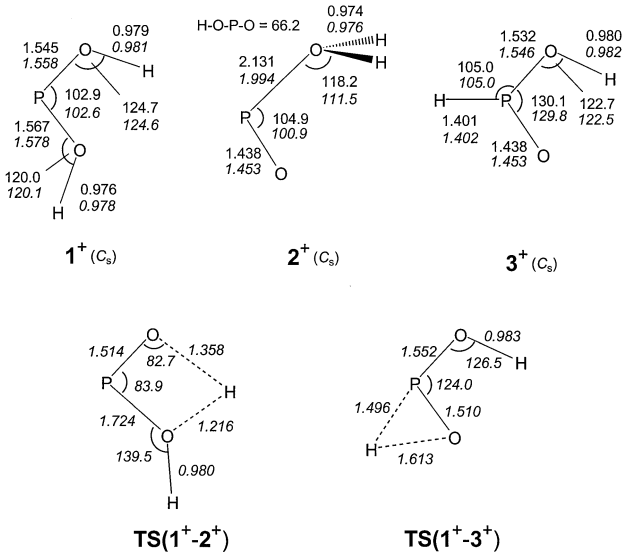

Figure 5. B3LYP optimized ion structures. Roman numerals: 6–311+G(2d,p) basis set, italic numerals 6–31G(d,p) basis set.

tion, collisions with CO_2 molecules under CI conditions are likely to dissipate the excess energy in the ions formed. Fully thermalized ions $\mathbf{1}^+$ have 17 kJ mol^{-1} mean internal energy at the ion source temperature of 523 K. The $[P,O_2,H_2]^+$ ion formed by CE showed a CID spectrum that was closely similar to that of ***A*** and ***C***. However, the NR spectrum differed substantially from those of ***A***–***C***, as discussed later.

Note that the enthalpies of formation of **I** and **II** are unknown, and so the pertinent appearance energies for the formation of $\mathbf{1}^+$ from these precursors could not be calculated.

Ion Structures and Energetics

To interpret the experimental data from ion dissociations, we investigated by calculations the potential energy surface for dissociations and isomerizations of $\mathbf{1}^+$–$\mathbf{3}^+$. The results from B3LYP calculations are summarized diagrammatically in Figure 4, the optimized ion structures are shown in Figure 5. Ion $\mathbf{1}^+$ is the most stable structure of the three studied. Structure $\mathbf{1}^+$ has a C_s symmetry with a syn-anti arrangement of the O—H bonds that corresponds to the lowest-energy orientation of the corresponding bond dipoles. Ion $\mathbf{2}^+$ is the second most stable structure, 84 kJ mol^{-1} less stable than $\mathbf{1}^+$ by G2 (Table 1). The P—OH_2 bond in $\mathbf{2}^+$ is about 25 % longer than a standard P—O bond (e.g., in $\mathbf{1}^+$), indicating a preferred dissociation to PO^+ and water which requires 121 kJ mol^{-1} by G2. Ions $\mathbf{1}^+$ and $\mathbf{2}^+$ are separated by an energy barrier (105 kJ mol^{-1} above $\mathbf{2}^+$ by B3LYP), which is below the lowest dissociation threshold for the formation of $PO^+ + H_2O$ (Figure 4). Ion $\mathbf{3}^+$ is 115 kJ mol^{-1} less stable than $\mathbf{1}^+$ (by G2) and is separated from the latter by an energy barrier (188 kJ mol^{-1} above $\mathbf{3}^+$ by B3LYP), which is substantially above the lowest dissociation threshold. Hence, non-dissociating $\mathbf{1}^+$ and $\mathbf{3}^+$ should not isomerize, and the less stable isomer $\mathbf{3}^+$ might be accessible by an ion chemistry synthesis in the gas phase.

The calculated energies imply that $\mathbf{1}^+$ and $\mathbf{2}^+$ of sufficient internal energies can isomerize prior to dissociation and display similar MI and CID spectra. Moreover, a fraction of non-dissociating $\mathbf{1}^+$ and $\mathbf{2}^+$ falling to the internal energy interval of ca. 163–200 kJ mol^{-1} can interconvert; note that such an isomerization should greatly favor the more stable isomer $\mathbf{1}^+$. MI dissociations of $\mathbf{3}^+$ should favor loss of water, which requires a rate-determining isomerization to $\mathbf{1}^+$, which should affect the dissociation kinetics and kinetic energy release. The other dissociations of $\mathbf{3}^+$ are substantially more endothermic, e.g., the cleavage of the H—P bond forming $O{=}POH^{+\cdot}$ that requires 381 or 360 kJ mol^{-1} by G2(MP2) or B3LYP, respectively. Nevertheless, a fraction of $\mathbf{3}^+$ that acquired high internal energy by collisional activation can be expected to undergo loss of H (a simple bond cleavage) competitively with elimination of water (a rearrangement). These properties are indic-

Table 1. Ion Relative Energies

	Relative energy[a]			
Species	B3LYP[b]	B3-MP2[c]	G2 (MP2)	G2
$\mathbf{1}^+$	0	0	0	0
$\mathbf{2}^+$	59	76	82	84
$\mathbf{3}^+$	134	102	115	115
TS ($\mathbf{1}^+ \rightarrow \mathbf{2}^+$)	163	–	–	–
TS ($\mathbf{1}^+ \rightarrow \mathbf{3}^+$)	322	–	–	–
TS ($\mathbf{2}^+ \rightarrow \mathbf{3}^+$)	339	–	–	–
$PO^+ + H_2O$	230	201	202	205
$POH^{+\cdot} + OH^{\cdot}$	481	514	509	507
$O{=}P\text{-}OH^{+\cdot} + H^{\cdot}$	494	508	494	496
$HPO^{+\cdot} + OH^{\cdot}$	594	–	–	–
$PO^{\cdot} + H_2O^{+\cdot}$	594	–	–	–

[a]In units of kJ mol^{-1} at 0 K.
[b]Calculations with the 6-31G(d,p) basis set.
[c]Calculations with the 6-311+G (3df,2p) basis set.

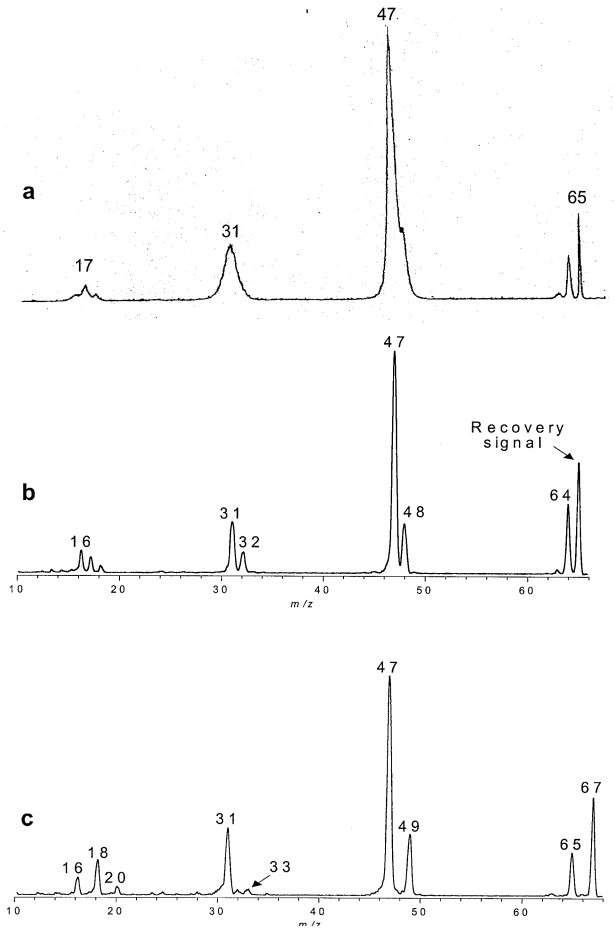

Figure 6. $^{+}NR^{+}$ mass spectra of ions ***B*** and [$^{2}H_2$]-***B***. (**a**) Ion ***B***, Xe, 70 % T/O_2, 70 % T. (**b**) Ion ***B***, CH_3SSCH_3, 70 % T/O_2, 70 % T. (**c**) Ion [$^{2}H_2$]-***B***, CH_3SSCH_3, 70 % T/O_2, 70 % T.

ative of the presence of structure $\mathbf{3}^{+}$ in ion ***B*** from diethyl phosphite. The ion relative energies further indicate that the $CO_2^{+\cdot}$ charge-exchange ionization of triethyl phosphite should produce the most stable isomer $\mathbf{1}^{+}$ exclusively, because the other isomers are energetically inaccessible. Ions ***A***–***C*** from the various precursors were further characterized by neutralization-reionization mass spectra that are discussed next.

Preparation and Dissociations of [P,O_2,H_2]· Radicals

The neutralization (Xe, 70 % T)-reionization (O_2, 70 % T) mass spectrum of ion ***A*** shows a rather weak survivor ion of reionized [P,O_2,H_2] at *m/z* 65 (Figure 1c). The major dissociations are nominally similar to those in the CID spectrum and include losses of H, OH, and H_2O, forming *m/z* 64, 48, and 47, respectively, the complementary *m/z* 17 and 18 species, and the peak of P at *m/z* 31. The relative intensities of the NR dissociation products are similar to those in the CID spectrum of ***A***, with a somewhat greater proportion of small fragments at *m/z* 16–18, and 31. The presence of the $H_2O^{+\cdot}$ ion in the NR spectrum can be in part due to CID of ion ***A*** upon collision with Xe, as the molecule of neutral water eliminated from ion ***A*** would be transmitted together with the neutralization products, reionized, and detected. Note that elimination of water from ion ***A*** is a major dissociation upon CID.

Table 2. [P,O_2,H_2] Ionization energies

Species		Energy[a] B3LYP[b]	B3-PMP2[c]	G2(MP2)	G2
1a	IE_a[d]	–	7.01	7.07	7.10
	IE_v[e]	–	7.75	7.63	–
	RE_v[f]	6.67	6.82	6.68	–
1b	IE_a	7.11	7.07	7.00	7.03
	IE_v	8.13	7.79	7.65	–
	RE_v	6.67	6.82	6.68	–
2	IE_a	6.96	7.27	7.18	7.23
	IE_v	7.51	7.61	7.50	–
	RE_v	6.44	7.03	6.90	–
3	IE_a	8.25	8.24	8.15	8.18
	IE_v	9.43	9.52	9.34	–
	RE_v	6.67	6.25	5.59	–

[a]In units of electron volt.
[b]Calculations with the 6–31 G(d,p) basis set.
[c]Calculations with the 6-311+G(3df,2p) basis set.
[d]Adiabatic ionization energy including zero-point vibrational corrections.
[e]Vertical ionization energy.
[f]Vertical recombination energy of the ion.

Neutralization of ion ***B*** was performed by collisions with Xe and CH_3SSCH_3. According to the calculated recombination energies of ion structures $\mathbf{1}^{+}$–$\mathbf{3}^{+}$ (Table 2), electron transfer from Xe (IE = 12.13 eV) is 4–5 eV endothermic, which can cause excitation in the radicals formed [70], while electron transfer from CH_3SSCH_3 (IE_a = 8.2 eV [71], IE_v = 8.96 eV) [72], is more closely energy balanced. The Xe/O_2 NR spectrum of ion ***B*** shows a substantially more abundant recovery ion at *m/z* 65, indicating a greater fraction of non-dissociating radicals reaching the reionization cell (Figure 6a). The CH_3SSCH_3/O_2 NR spectrum of ion ***B*** shows even greater relative abundance of the recovery ion which amounts to 50 % of the *m/z* 47 base peak (Figure 6b). Another distinguishing features of the NR spectrum of ***B*** are the [*m/z* 64]/[*m/z* 65] ratio and the increased relative abundance of the HP^{+} ion at *m/z* 32.

Deuterium labeling (ion [$^{2}H_2$]-***B***, Figure 6c) basically confirms the product assignments through the corresponding mass shifts due to the presence of deuterium atoms. Loss of D (*m/z* 65) and formation of PD (*m/z* 33) show isotope effects compared with the corresponding loss of H and formation of PH from ion ***B***. However, there is a negligible isotope effect on the relative abundance of the recovery ion (*m/z* 67).

In order to distinguish intrinsic dissociations of [P,O_2,H_2] radicals from those of ions ***B***, we performed variable-time NR measurements for neutralization with CH_3SSCH_3 and reionization with O_2 that provided rate parameters for the neutral and post-reionization ion dissociations (Table 3). The rate parameters clearly show that both radicals and ions undergo dissociations

Table 3. Rate parameters for radical and ion dissociations from variable-time NR spectra

	Rate parameters (10^6 s^{-1})	
Dissociation[a]	k_N	k_i
$[P,O_2,H_2] \rightarrow$ **OPOH** + H	0.14	0.25
$[P,O_2,H_2] \rightarrow$ **POH** + OH	0.17	0.45
$[P,O_2,H_2] \rightarrow$ **PO** + H_2O	0.45	1.07

[a]The species given in bold characters were measured in the observation channel.

forming products at the same *m/z* values. The temporal differentiation of the neutral and ion dissociations further shows that the latter account for 73 % of loss of OH, 70 % loss of water, and 64 % loss of H. In summary, the NR spectra are dominated by post-reionization dissociations of $[P,O_2,H_2]^+$ cations.

The CH_3SSCH_3/O_2 NR spectrum of ion ***C*** was similar to that of ion ***B***, except for a small difference in the relative abundances of the *m/z* 64, 32, and 17 ions (Figure 7). To investigate the effect of precursor ion internal energy, we obtained an NR mass spectrum of ion ***C*** prepared by the charge-exchange dissociative ionization of triethyl phosphite, which should produce ***C*** with nearly thermal internal energies. The spectrum shows a dramatically increased abundance of the recovery ion which becomes the dominant peak in the spectrum (Figure 7b). The dissociation products show relative abundances that are similar to those in Figure 7a and also those in the CID spectrum of ion ***C***. The energy effects in the NR spectra and the radical isomers formed are further discussed with the help of ab initio and RRKM calculations.

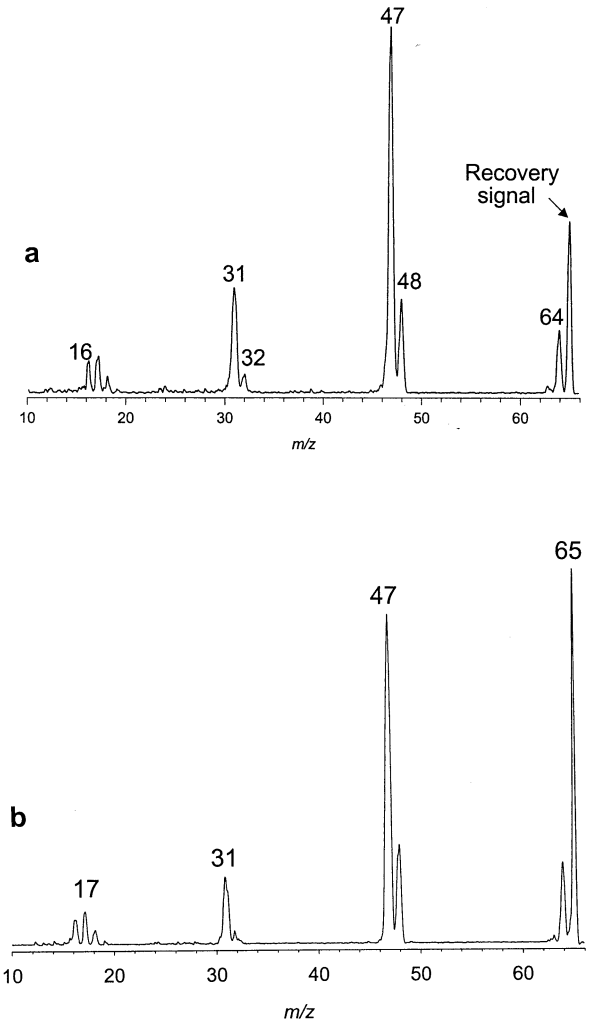

Figure 7. $^+NR^+$ mass spectra of ion ***C***. (**a**) Ion ***C*** by 70-eV electron ionization, CH_3SSCH_3, 70 % T/O_2, 70 % T. (**b**) Ion ***C*** by charge-exchange ionization, CH_3SSCH_3, 70 % T/O_2, 70 % T.

Radical Structures and Energetics

Geometry optimizations found two local minima for the dihydroxyphosphinyl radical. The syn-anti rotamer (**1a**) was marginally more stable than the anti-anti rotamer (**1b**)(Figure 8), and the rotamers were separated by a small potential energy barrier that disappeared upon ZPVE correction. Hence, rotamers **1a** and **1b** can be viewed as a fluxional structure (**1**) with free rotations about the P—O bonds. Radical **2** was a local energy minimum that was 73–80 kJ mol^{-1} less stable than **1** (Figure 9). **2** had a long P—OH_2 bond (2.49 Å) that indicated facile dissociation to $PO^{\cdot}$ and water. Indeed, the 0 K bond dissociation energy was calculated at 15–18 kJ mol^{-1}, indicating only a marginal stability for **2**. Structures **1** and **2** were separated by a substantial energy barrier (**TS4** in Figure 9) that was 138–142 kJ mol^{-1} above 1 and 43–46 kJ mol^{-1} above $PO^{\cdot}$ + H_2O.

In contrast to the cation relative stabilities, radical **3** was only slightly less stable than **1** and should represent a kinetically stable isomer. Radicals **1** and **3** were separated by a large energy barrier for hydrogen migration (**TS1**, Figure 9) that was 161–164 kJ mol^{-1} above **1**.

The threshold energies for product formation indicated elimination of water and loss of H as the two most favorable dissociations. Cleavage of the H—P bond in **3** was continuously endothermic in B3LYP calculations and did not show a saddle point above the threshold energy of the products. Hence radical **3** is bound by 110–118 kJ mol^{-1} at our highest levels of theory. Cleavage of the anti-H—O bond in **1** proceeded through a transition state (**TS2**) that was 35–44 kJ mol^{-1} above the thermochemical threshold for O=P—OH + $H^{\cdot}$. This should provide an additional stabilization for **1** and also affect the kinetics of H atom addition to phosphorous acid. The potential energy diagram in Figure 9 indicates the most favorable dissociations of the phosphorus radicals. **1** and **2** should prefer dissociation to $PO^{\cdot}$ + H_2O, whereas **3** should prefer losing the P-bound hydrogen atom.

The internal energy needed to drive these dissociations can be provided by Franck-Condon effects on vertical electron capture by the corresponding cations.

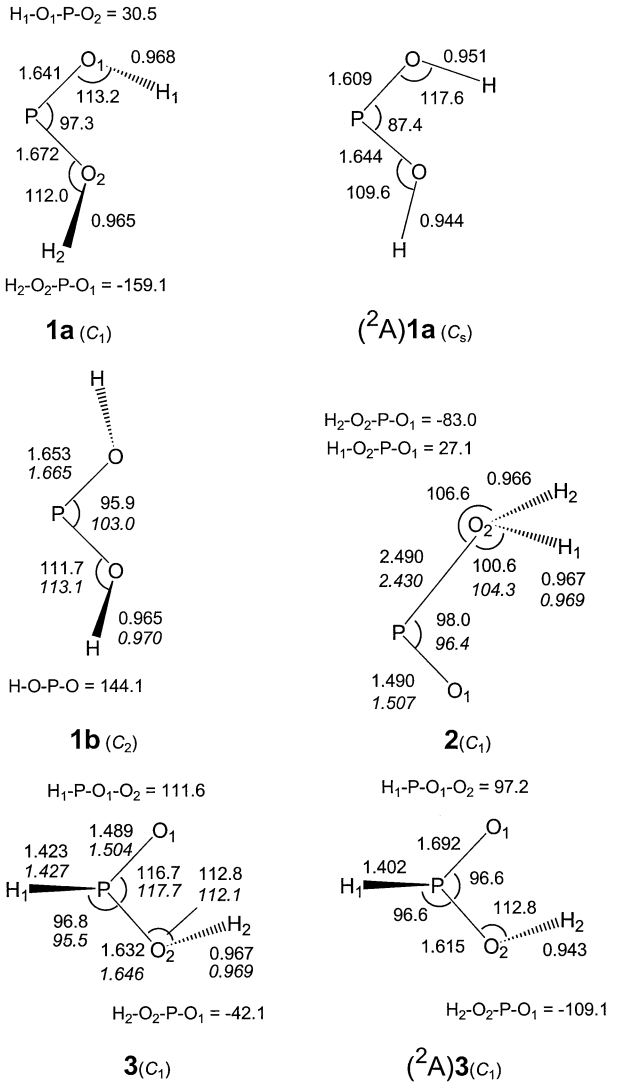

Figure 8. B3LYP optimized neutral structures. Roman numerals: 6–311 + G(2d,p) basis set, italic numerals 6–31G(d,p) basis set.

For **1**, the Franck-Condon energy (33 kJ mol^{-1}) alone was insufficient to cause dissociation. In contrast, vertical neutralization of $\mathbf{2}^+$ forms **2** with an internal energy close to the dissociation threshold indicating facile dissociation. The Franck-Condon energy in vertically formed **2** originates mostly from the compression of the P—OH_2 bond which is 0.36 Å shorter in $\mathbf{2}^+$ than in the relaxed geometry of the radical.

Interestingly, vertical electron capture in $\mathbf{3}^+$ results in large Franck-Condon effects, such that **3** is formed with 70 kJ mol^{-1} above the dissociation threshold. Such a large vibrational excitation should result in fast dissociation (see below) preventing detection of **3** on a microsecond time scale. The Franck-Condon energy in vertically formed **3** stems from the combined effects of P—O and P—H bond compression and planarization at phosphorus in the ion, while the radical is pyramidized.

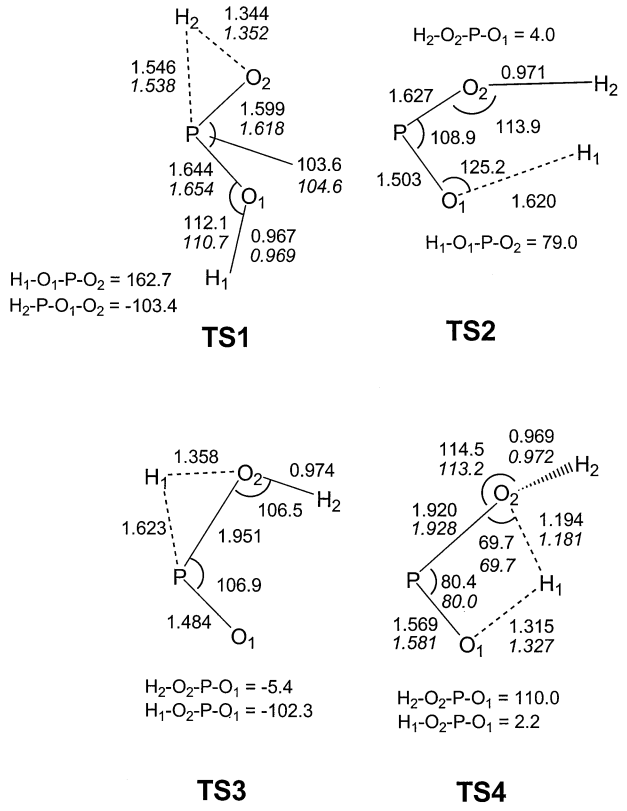

Figure 8b (continued)

RRKM Dissociation Kinetics—Comparison with Experiment

The calculated transition state energies allowed us to evaluate the unimolecular dissociation kinetics of the most stable radical **1** using RRKM calculations. The unimolecular rate constants for loss of H, isomerization to **2**, and isomerization to **3** are shown in Figure 10.

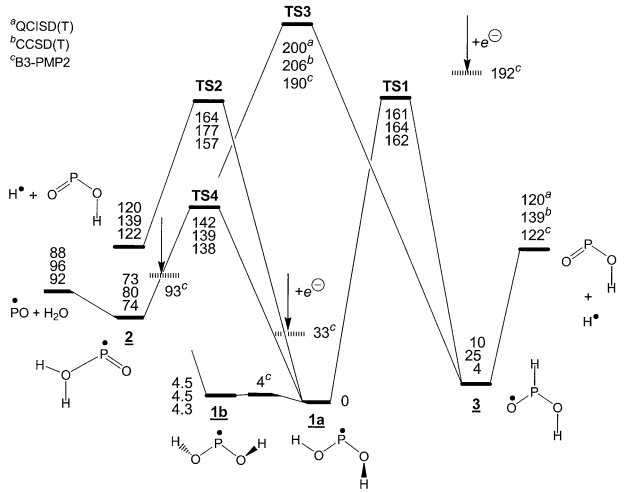

Figure 9. Potential energy surface for [P,O_2,H_2] radicals. Relative energies at 0 K from (top, **a**) QCISD(T)/6–311 + G(3df,2p), (middle, **b**) CCSD(T)/aug-cc-pVTZ, and (bottom, **c**) B3-PMP2/6–311 + G(3df,2p) single-point calculations and B3LYP/6–311 + G(2d,p) zero-point corrections.

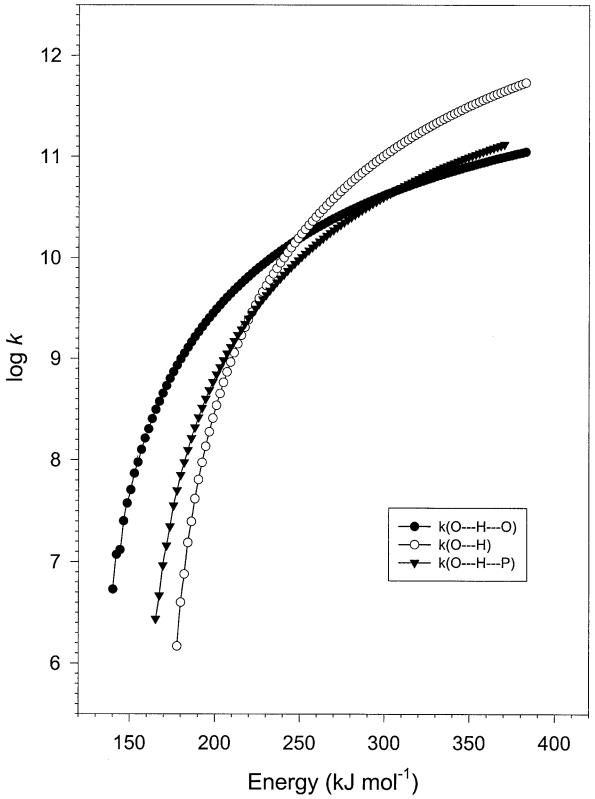

Figure 10. RRKM rate constants for dissociations of **1**. CCSD(T)/aug-cc-pVTZ energies and B3LYP/6–311 + G(2d,p) harmonic frequencies, zero-point energies, and moments of inertia.

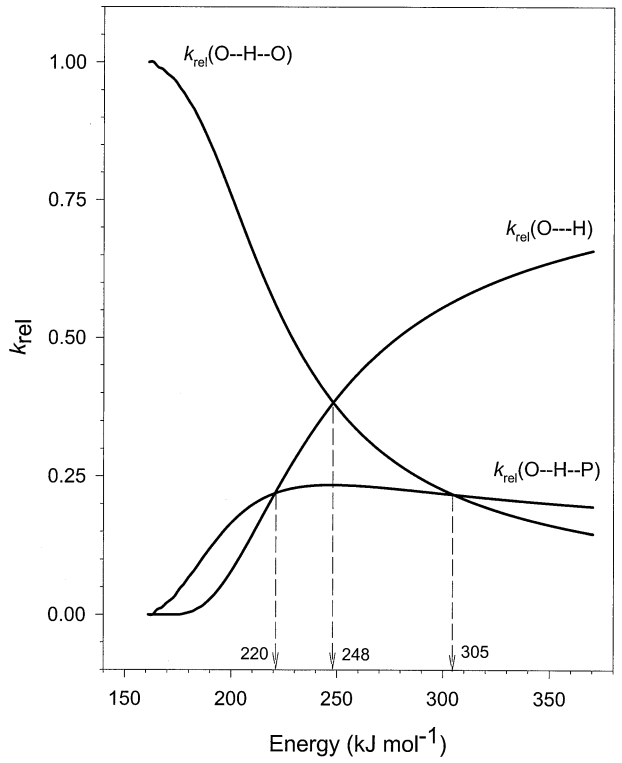

Figure 11. RRKM branching ratios for loss of H_2O and H from **1**.

These rate constants are based on CCSD(T)/aug-cc-pVTZ transition state energies; RRKM calculations using QCISD(T) and B3-PMP2/6–311 + G(3df,2p) energies gave similar results that are not discussed separately. Isomerization to **2** is the lowest-energy process that should dominate the unimolecular chemistry of **1** in the energy interval of 139–248 kJ mol^{-1}. Since the **TS4** energy is above the dissociation threshold for $PO^{\cdot}$ + H_2O, **2** formed by isomerization is expected to dissociate rapidly, so that the isomerization is the rate determining step for the overall dissociation **1** → **2** → $PO^{\cdot}$ + H_2O. Compared with the latter reaction, the processes that can lead to loss of H are substantially slower at internal energies <248 kJ mol^{-1}. The **1** → **3** isomerization, followed by dissociation to O=P—OH + $H^{\cdot}$, is faster than direct loss of H from **1** at internal energies up to 220 kJ mol^{-1} where the *k* curves cross. The **1** → **3** isomerization overtakes that for **1** → **2** at 305 kJ mol^{-1} excitation. The calculations thus indicate that at intermediate excitations, **1** should dissociate exclusively by loss of water. In addition, because of the small number of degrees of freedom in **1**, the log *k* curves increase rapidly with internal energy, such that the rate constants exceed 10^6 s^{-1} within 1–2 kJ mol^{-1} above the TS.

Are the calculated potential energy surface and RRKM rate constants compatible with the experimental results? The energy analysis indicates that ion ***C*** prepared by CE ionization of triethyl phosphite was pure $\mathbf{1}^+$. Its internal energy consists of that of the precursor ion and that due to Franck-Condon effects on vertical electron transfer, e.g., $E_{int}(\mathbf{1})$ = 17 + 33 = 50 kJ mol^{-1}. This energy is insufficient to cause dissociation of **1**, in keeping with the low extent of fragmentation and abundant recovery ion in the NR mass spectrum (Figure 7). The dissociation products observed in the Figure 7 NR mass spectrum can be assigned to post-reionization ion dissociations, in keeping with the close resemblance of the fragmentation patterns in the NR and CID spectra of the same ion. NR dissociations of ion ***C*** prepared by 70-eV dissociative ionization also show a dominant proportion of ion processes, as determined by variable-time measurements. However, radical dissociations also occur and show relative rate parameters, k_{rel} = 0.60, 0.14, and 0.25, for the loss of water, H, and OH, respectively. These are in qualitative agreement with the branching ratios obtained from RRKM calculations. Figure 11 shows that a 0.60:0.14 ratio for the loss of water following rate-determining isomerization to **2**, k_{rel}(O–H–O), and combined losses of H due to a direct loss, k_{rel}(O–H), and rate-determining isomerization to **3**, k_{rel}(O–H–P), is achieved at 195 kJ mol^{-1} excitation in **1**. However, at this excitation, the RRKM rate constants are in the 10^8–10^9 s^{-1} range and could not account for dissociations occurring on the 0.4–3.8 μs time scale which is probed by the variable-time measurements. In addition, the threshold energy for the loss of $OH^{\cdot}$ from **1** is calculated as 312 kJ mol^{-1} for the lowest threshold of (^{1}A') H–P=O + $OH^{\cdot}$ (Table 4), so that no loss of $OH^{\cdot}$

Table 4. Relative energies of $[P,O_2,H_2]$ radicals

Species	Relative energy[a]					
	B3LYP[b]	B3-PMP2[c]	G2(MP2)	G2	QCISD(T)[c]	CCSD(T)[d]
1a	–	0	0	0	0	0
1b	0	4.3	6.5	6.7	4.5	4.5
TS(1a → 1b)	–	3.7	3.8	4.1	–	–
2	75	74	70	72	73	80
3	25	4	11	11	10	25
TS1	171	162	160	161	161	164
TS2	–	157	163	160	164	177
TS3	188	190	199	200	200	206
TS4	130	138	141	142	142	139
$PO^{\cdot} + H_2O$	109	92	77	62	88	96
$O{=}P\text{-}OH + H^{\cdot}$	151	122	122	123	120	139
$(^1A')H\text{-}P{=}O + OH^{\cdot}$	310	319	308	306	304	312
$(^1A')P\text{-}OH + OH^{\cdot}$	444	476	–	–	–	–
$(^3A'')P\text{-}OH + OH^{\cdot}$	–	393	399	395	379	

[a]In units of kJ mol^{-1} at 0 K.
[b]Calculations with the 6–311G(d,p) basis set.
[c]Calculations with the 6–311+G(3df,2p) basis set.
[d]Calculations with the aug-cc-pVTZ basis set.

should occur at 195 kJ mol^{-1}, contradicting the experimental data.

The NR spectra of ions ***A*** and ***B*** allow one a somewhat less unambiguous interpretation because of the possible presence of the less stable isomers **2** and **3**. For NR of ion ***A***, internal energy effects can account for the increased dissociation of the intermediate $[P,O_2,H_2]^{\cdot}$ radicals and reionized ***A***. However, if $\mathbf{2}^+$ was co-formed by dissociative ionization of methylphosphonic acid, its neutralization should result in rapid dissociation by loss of water which would decrease the relative abundance of the survivor ion, as observed. With NR of ion ***B***, the increased relative abundance of the *m/z* 64 fragment points to a loss of H from the neutral intermediate.§ The potential energy diagram (Figure 9) indicates that loss of H should be the dominant dissociation of **3**, especially following vertical neutralization that forms the radical with a large excess of internal energy. The NR spectrum of ion ***B*** thus can be interpreted as resulting from the presence of stable isomers $\mathbf{1}^+/\mathbf{1}$ that provide the recovery ion and dissociate mainly by loss of water, and the less stable ion $\mathbf{3}^+$ that upon neutralization produces an unstable radical **3** that dissociates completely by loss of H.

*Excited Electronic States of **1** and **3***

In order to explain the unusual branching ratios in dissociations of **1** one needs to consider a mechanism by which the radical acquires internal energy upon vertical electron transfer. As discussed above, Franck-Condon effects alone are insufficient to trigger the radical dissociations. As shown previously, collisional electron transfer can lead to the formation of excited electronic states in the neutral species that accepted the electron. With even electron ions in particular, this can occur by electron capture in the manifold of unoccupied orbitals, or by excitation of a valence electron from the closed shell. The excited electronic states that have short (<ns) radiative lifetimes will emit a photon and decay to the ground state without affecting the dissociation kinetics. However, long-lived excited states of μs lifetimes (denoted as the dark states) [73] can undergo dissociations on the excited state PES or funnel the electronic energy into vibrational excitation of the ground state by internal conversion through avoided crossings or conical intersections. Ground-electronic state radicals formed by internal conversion from an excited state will have internal energies which are centered about the electronic excitation energy and shifted and broadened by the ion vibrational energy and Franck-Condon effects. Although here we did not investigate excited states in **1**-**3** experimentally [74], we performed time-dependent

Table 5. Excited electronic states in **1** and **3**

Species	State	Excitation energy[a]			τ[b]		
		(X)[c]	(A)[d]	($\mathbf{1}^+$)[e]	(X)	(A)	($\mathbf{1}^+$)
1a	A	2.85	2.61	2.81	7	22	2
	B	3.52	3.95	3.06	0.3	0.2	0.8
	C	4.40	4.60	4.28	0.05	0.07	0.07
3	A	3.36	1.31	2.63	0.8	>30	3.3
	B	3.89	2.61	4.24	0.08	0.3	>30
	C	4.95	3.92	4.80	0.06	0.07	0.07

[a]From TD-B3LYP/6–311+G(3df,2p) calculations in units of electronvolt.
[b]Radiative lifetimes (μs) for vertical transitions.
[c]Vertical excitations from the B3LYP/6-311+G(2d,p) optimized geometry of the ground state.
[d]Adiabatic excitation energies from the UCIS/6-311+G(2d,p) optimized geometry of the first excited state.
[e]Adiabatic excitation energies from the B3LYP/6-311+G(2d,p) optimized geometry of the ion.

§ As opposed to an ion internal energy effect on post-reionization dissociations. CAD relative intensities of ions produced by high-energy dissociations are insensitive to the precursor ion internal energy.

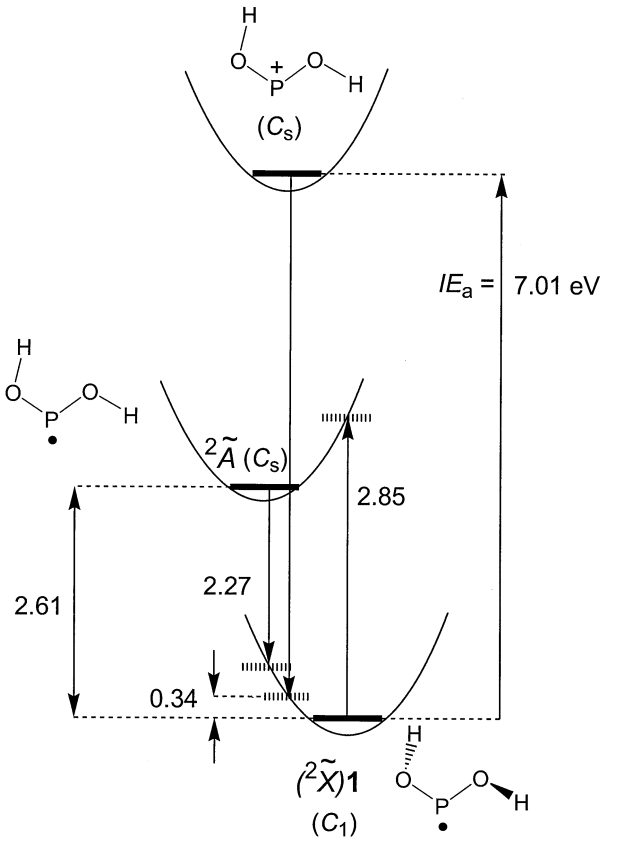

Figure 12. Excited state potential energy surfaces in **1**.

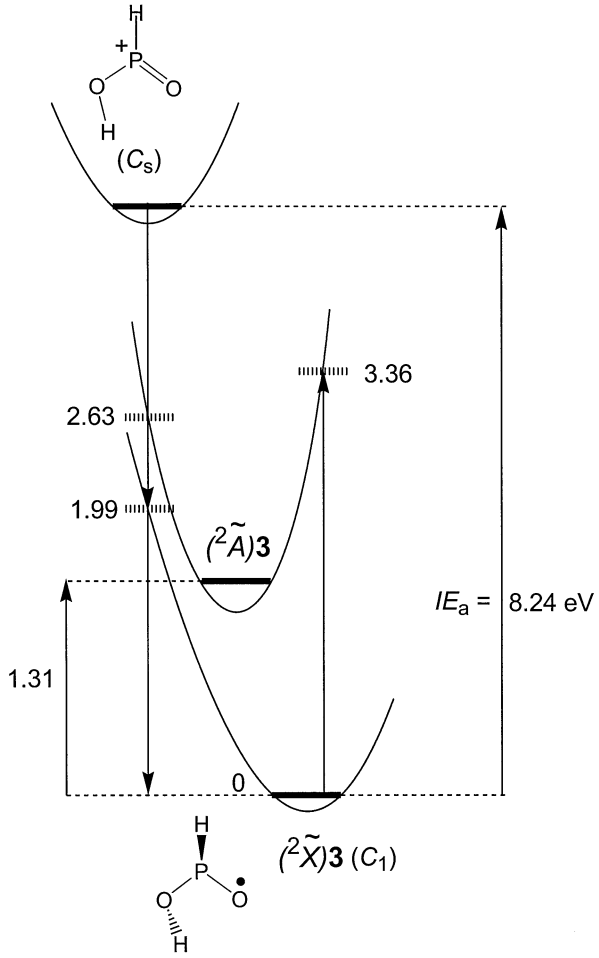

Figure 13. Excited state potential energy surfaces in **3**.

density functional theory calculations to shed some light on the relevant excitation energies and radiative lifetimes.

The first two excited states in **1a** are long lived and therefore kinetically relevant. The *A* state excitation energy (2.81 eV in vertically formed radical, Table 5) is sufficient to promote rearrangements to **2** and **3**, and loss of H, but not the loss of OH. At this excitation energy, k_{rel}(O–H) + k_{rel}(O–H–P) > k_{rel}(O–H–O), so that the total loss of H exceeds the loss of water. The *B* state excitation energy (3.06 eV, Figure 12) is just below the threshold for HP=O + $OH^{\cdot}$; in order for the loss of OH to occur, the requisite energy must be provided by the *C* or a higher excited state.

The μs kinetics for the loss of H and water can now be explained by a combination of energy effects originating from the ground and excited states. **1** produced in the *X* state will have internal energies E_{int} >33 kJ mol^{-1} depending on the internal energy of the precursor ion. Radicals of sub-threshold E_{int} are stable; those with $E_{int} \geq E$(**TS4**) dissociate by loss of water. **1** produced in the *A* and *B* states undergo rate-determining internal conversion to the *X* state that occurs on the μs time scale. The energy which is funneled into (*X*)**1** causes very rapid competing dissociations via **TS1**, **TS2** and **TS4** with rate constants $>10^9$ s^{-1} (Figure 10) and branching ratios shown in Figure 11. The variable-time measurements average the processes occurring on the μs time scale by monitoring the dissociation products.

The *A* and *B* states of **3** also have microsecond radiative lifetimes (Table 5). Electron capture to form the *A* state is accompanied by Franck-Condon effects that amount to ca 130 kJ mol^{-1}. From the energy difference between the equilibrium geometries of the *X* and *A* states (1.31 eV) and that between the vertical landing points on the corresponding potential energy surfaces (2.63–1.99 = 0.64 eV) it follows that the *X* and *A* surface are close at the Franck-Condon excitation (Figure 13). This should enhance the coupling elements for internal conversion [75] and decrease the *A* state lifetime. Since the *X* state acquires 2.63 eV from internal conversion, it should dissociate rapidly by H atom loss. This means that an increased probability for internal conversion to the dissociative *X* state can be expected to diminish the lifetime of vertically produced **3**, but should not change the unimolecular chemistry.

Conclusions

Dissociative ionization of triethylphosphite under charge-exchange conditions that provide energy control

generates the most stable $[P,O_2,H_2]^+$ isomer, dihydroxyphosphonium cation $\mathbf{1}^+$, that affords stable dihydroxyphosphonium radical (**1**) by collisional electron transfer. When formed from a more energetic cation, the radical undergoes dissociations and isomerizations that were quantified by variable-time measurements and explained by theory. Cations produced by dissociative ionization of methylphosphonic acid and diethyl phosphite consist mostly of $\mathbf{1}^+$ but also contain the less stable isomers $\mathbf{2}^+$ and $\mathbf{3}^+$, respectively. The transient formation of **3** is deduced from its NR dissociation by loss of H, as explained by theory. The branching ratios for loss of H and water from **1** occurring on the microsecond time scale are interpreted by a combination of rate-determining internal conversion from excited electronic states promoting fast loss of H and direct elimination of water from metastable **1** that occurs entirely on the ground state potential energy surface.

Acknowledgments

The authors thank Dr. K. V. Raghavan, Director, IICT, Hyderabad, for facilities, and Dr. M. Vairamani and Dr. B.M. Choudary for cooperation. RSKthanks CSIR, New Delhi, for the award of Junior Research Fellowship. KBP thanks DST, New Delhi for the funding. Research at the University of Washington was supported by grants from the National Science Foundation, CHE-0090930 for instrumentation and CHE-9808182 for the Computational Chemistry Center, the latter jointly with the University of Washington.

References

1. Cowley, A. H. Stable Compounds with Double Bonding Between the Heavier Main-Group Elements. *Acc. Chem. Res.* **1984,** *17,* 386–392.
2. Cowley, A. H. Double Bonding Between the Heavier Main-Group Elements: From Reactive Intermediates to Isolable Molecules. *Polyhedron* **1984,** *3,* 389–432.
3. Schoeller, W. W. Bonding Properties of Low Coordinated Phosphorus Compounds. In: *Multiple Bonds and Low Coordination in Phosphorus Chemistry*, Regitz, M.; Scherer, O., Eds.; Georg Thieme Verlag: Stuttgart, 1990. Chapter B, pp. 5–32.
4. Scherer, O. J. Phosphorus, Arsenic, Antimony, and Bismuth Multiply Bonded System with Low Coordination Number: Their Role as Complex Ligands. *Agnew. Chem. Int. Ed. Engl.* **1985**, *97*, 905, 924–943.
5. Sanchez, M.; Mazieres, M. R.; Lamande, L.; Wolf, R. Phosphenium Cations. In: *Multiple Bonds and Low Coordination in Phosphorus Chemistry*, Regitz, M.; Scherer, O., Eds.; Georg Thieme Verlag, Stuttgart, 1990, Chapter D, pp. 129–148.
6. Kruger, G. J.; Lotz, S.; Linford, L.; Vandtk, M.; Raubenheimer, H. G. Sulfur-Containing Metal-Complexes. 23. Synthesis of New Complexes Containing the $Fe_2(CO)_6S_2$ Butterfly Unit. Crystal and Molecular Structure of $[Fe_2(CO)_6(\eta$-$S_2P(C_6H_4OMe$-$P)Fe(CO)_4]$, Determined from Two Different Crystal Modifications. *J. Organomet. Chem.* **1985,** *280,* 241–251.
7. Lindner, E.; Auch, K.; Weiss, G. A.; Hiller, W.; Fawzi, R. Preparation and Properties of, and Reactions with, Metal-Containing Heterocycles. 53. Stabilization of Thiophosphanes and Dithiophosphoranes with Carbonyl Metal-Complexes. *Chem. Ber.* **1986,** *119,* 3076–3088.
8. Wesdemiotis, C.; McLafferty, F. W. Neutralization Reionization Mass Spectrometry (NRMS). *Chem. Rev.* **1987,** *87,* 485–500.
9. Holmes, J. L. The Neutralization of Organic Cations. *Mass Spectrom. Rev.* **1989,** *8,* 513–539.
10. Tureček, F. The Modern mass Spectrometer. A Laboratory for Unstable Neutral Species. *Org. Mass Spectrom.* **1992,** *27,* 1087–1097.
11. Zagorevski, D. V.; Holmes, J. L. Neutralization-Reionization Mass Spectrometry Applied to Organometallic and Coordination Chemistry. *Mass Spectrom. Rev.* **1994,** *13,* 133–154.
12. Goldberg, N.; Schwarz, H. Neutralization-Rreionization Mass Spectrometry. A Powerful Laboratory to Generate and Probe Elusive Neutral Molecules. *Acc. Chem. Res.* **1994,** *27,* 347–352.
13. Zagorevski, D. V.; Holmes, J. L. Neutralization-Reionization Mass Spectrometry Applied to Organometallic and Coordination Chemistry (update: 1914–1998). *Mass Spectrom. Rev.* **1999,** *18,* 87–118.
14. Keck, H.; Kuchen, W.; Renneberg, H.; Terlouw, J. K.; Visser, H. C. RS–P=S in the Gas Phase. First Generation of (Organothio)Thiophosphanes. *Angew. Chem. Int. Ed. Engl.* **1991,** *30,* 318–320.
15. Keck, H.; Kuchen, W.; Renneberg, H.; Terlouw, J. K. On the Existence of H_3PS and its Radical Cation in the Gas Phase. *Phosphorus. Sulfur Rel. Elem.* **1988,** *40,* 227–232.
16. Keck, H.; Kuchen, W.; Renneberg, H.; Terlouw, J. K.; Visser, H. C. Gaseous H_3PS_2. Generation and Characterization. *Z. Anorg. Allg. Chem.* **1990,** *580,* 181–187.
17. Wong, T.; Terlouw, J. K.; Keck, H.; Kuchen, W.; Tommes, P. The Thioxophosphane H–P=S and its tautomer H–S–P, (Thiohydroxy)Phosphinidene, are Stable in the Gas Phase. *J. Am. Chem. Soc.* **1992,** *114,* 8208–8210.
18. Gu, M.; Tureček, F. The Precursor Scan. A New Type of Experiment in Neutralization-Reionization Mass Spectrometry. *Org. Mass Spectrom.* **1993,** *28,* 1135–1143.
19. Vivekananda, S.; Srinivas, R. Generation and Characterization of Ionic and Neutral (Methylthio)Oxophosphane $(CH_3S–P=O)^{+\cdot/o}$ and (Methoxy)Oxophosphane $(CH_3O–P=O)^{+\cdot/o}$ by Neutralization-Reionization Mass Spectrometry. *Int. J. Mass Spectrom. Ion Processes* **1997,** *171,* 79–82.
20. Vivekananda, S.; Raghunath, P.; Bhanuprakash, K.; Srinivas, R. Characterization of Ammonia Phosphorus Oxide H_3NPO^+ Ions and Their Neutral Counterparts by Mass Spectrometry and Computational Chemistry. *Int. J. Mass Spectrom.* **2001,** *208,* 59–65.
21. Tureček, F.; Gu, M.; Hop, C. E. C. A. Franck-Condon Dominated Chemistry. Formation and Dissociations of Tetrahydroxyphosphoranyl Radicals Following Femtosecond Reduction of their Cations in the Gas Phase. *J. Phys. Chem.* **1995,** *99,* 2278–2291.
22. Gustafson, S. M.; Cramer, C. J. Ab initio Conformational and Stereopermutational Analyses of Phosphoranyl Radicals $HP(OR)_3$ and $P(OR)_4$ [R = H or CH_3]. *J. Phys. Chem.* **1995,** *99,* 2267–2277.
23. Cramer, C. J.; Gustafson, S. M. An ab initio Conformational and Stereopermutational Analysis of Dihydroxyphosphoranyl, $H_2P(OH)_2$. *J. Am. Chem. Soc.* **1994,** *116,* 723–734.
24. Cramer, C. J.; Gustafson, S. M. Hyperconjugation versus Apicophilicity in Trigonal Bipyramidal Phosphorus Species. *J. Am. Chem. Soc.* **1993,** *115,* 9315–9316.
25. Cramer, C. J. Where Is the Unpaired Electron in the Phosphoranyl Radicals H_3PS and H_3PSH? *Chem. Phys. Lett.* **1993,** *202,* 297–302.
26. Cramer, C. J. The Fluorophosphoranyl Series. Theoretical Insights into Relative Stabilities and Localization of Spin. *J. Am. Chem. Soc.* **1991,** *113,* 2439–2447.
27. Cramer, C. J. Theoretical Rotation, Pseudorotation, and Pseudoinversion Barriers for the Hydroxyphosphoranyl Radical. *J. Am. Chem. Soc.* **1990,** *112,* 7965–7972.

28. Cramer, C. J.; Dykstra, C. E.; Denmark, S. E. An ab initio Study of the [1, 2]. Proton Transfer from Phosphine Oxide to Phosphinic Acid. *Chem. Phys. Lett.* **1987,** *136,* 17–21.
29. Glidewell, C. Semiempirical MNDO SCF-MO Study of Radicals Derived from γ-Radiolysis of Tertiary Phosphines and Trialkylphosphites. *J. Chem. Soc. Perkin Trans. 2.* **1985**, 551–555.
30. Steiner, V.; Daoust-Maleval, I.; Tabet, J.-C. Study of Gas-Phase Reactivity of Positive and Negative Even-Electron Ions Prepared from Diethylmethyl Phosphonate Ester in an External Chemical Ionization Source of Orthogonal Tandem Quadrupole/Ion Trap Instrument. *Int. J. Mass Spectrom.* **2000,** *195/196,* 121–138.
31. Gudat, D. Cation Stabilities, Electrophilicities, and "Carbene Analog" Character of Low Coordinate Phosphorus Cations. *Eur. J. Inorg. Chem.* **1998**, 1087–1094.
32. McCombie, H.; Saunders, B. C.; Stacey, G. J. Esters Containing Phosphorus. Part I. *J. Chem. Soc.* **1945**, 380–382.
33. Cooks, R. G.; Beynon, J. H.; Caprioli, R. M.; Lester, G. R. *Metastable Ions.* Elsevier: Amsterdam, 1973; 60–62.
34. Holmes, J. L.; Terlouw, J. K. The Scope of Metastable Peak Observations. *Org. Mass Spectrom.* **1980,** *15,* 383–396.
35. Tureček, F.; Gu, M.; Shaffer, S. A. A Novel Tandem Quadrupole Acceleration-Deceleration Mass Spectrometer for Neutralization-Reionization Studies. *J. Am. Soc. Mass Spectrom.* **1992,** *3,* 493–501.
36. Kuhns, D. W.; Tran, T. B.; Shaffer, S. A.; Tureček, F. The Methylthiomethyl Radical. A Variable-Time Neutralization-Reionization and ab initio Study. *J. Phys. Chem.* **1994,** *98,* 4845–4853.
37. Kuhns, D. W.; Tureček, F. Unimolecular Neutral and Ion Kinetics by Variable-Time Neutralization-Reionization Mass Spectrometry. *Org. Mass Spectrom.* **1994,** *29,* 463–469.
38. Schmidt, M. W.; Baldridge, K. K.; Boatz, J. A.; Jensen, J. H.; Koseki, S.; Gordon, M. S.; Nguyen, K. A.; Windus, T. L.; Albert, S. T. *Quantum Chem. Prog. Exchange Bull.* **1990**, *10.*
39. Schmidt, M. W.; Baldridge, K. K.; Boatz, J. A.; Elbert, S. T.; Gordon, M. S.; Jensen, J. H.; Koseki, S.; Matsunaga, N.; Nguyen, K. A.; Su, S.; Windus, T. L. General Atomic and Molecular Electronic-Structure System. *J. Comput. Chem.* **1993,** *14,* 1347–1363.
40. Guest, M. F.; Van Lanhe, J. H.; Kendrik, J.; Scholtel, K.; Schorwood, P. with contributions from Amos, R. D.; Buenker, R. J.; Van Dam, H. J. J.; Dupuis, M.; Handy, N. C.; Hiller, I. H.; Knowles, J.; Bonacic-Koutecky, V.; Von Niessen, W.; Harison, R. J.; Rendell, A. P.; Saunders, V. R.; Stone, A. J.; de Vries, A. H. GAMESS-UK package of ab initio programs derived from the original GAMESS code attributable to Dupuis, M.; Spangler, D.; Wendolosia, J. NRCC Software Catalog, Vol. 1, Program No. QG 01 (GAMESS), 1980.
41. Frisch, M. J.; Trucks, G. W.; Schlegel, H. B.; Scuseria, G. E.; Robb, M. A.; Cheeseman, J. R.; Zakrzewski, V. G.; Montgomery, J. A.; Stratmann, R. E.; Burant, J. C.; Dapprich, S.; Millam, J. M.; Daniels, A. D.; Kudin, K. N.; Strain, M. C.; Farkas, O.; Tomasi, J.; Barone, V.; Cossi, M.; Cammi, R.; Mennucci, B.; Pomelli, C.; Adamo, C.; Clifford, S.; Ochterski, J.; Petersson, G. A.; Ayala, P. Y.; Cui, Q.; Morokuma, K.; Malick, D. K.; Rabuck, A. D.; Raghavachari, K.; Foresman, J. B.; Cioslowski, J.; Ortiz, J. V.; Stefanov, B. B.; Liu, G.; Liashenko, A.; Piskorz, P.; Komaromi, I.; Gomperts, R.; Martin, R. L.; Fox, D. J.; Keith, T.; Al-Laham, M. A.; Peng, C. Y.; Nanayakkara, A.; Gonzalez, C.; Challacombe, M.; Gill, P. M. W.; Johnson, B. G.; Chen, W.; Wong, M. W.; Andres, J. L.; Head-Gordon, M.; Replogle, E. S.; Pople, J. A. *Gaussian 98, Revision A.6*; Gaussian, Inc., Pittsburgh, 1998.
42. Becke, A. D. A New Mixing of Hartree-Fock and Local Density-Functional Theories. *J. Chem. Phys.* **1993,** *98,* 1372–1377.
43. Becke, A. D. Density-Functional Thermochemistry. 3. The Role of Exact Exchange. *J. Chem. Phys.* **1993,** *98,* 5648–5652.
44. Stephens, P. J.; Devlin, F. J.; Chabalowski, C. F.; Frisch, M. J. Ab initio Calculation of Vibrational Absorption and Circular Dichroism Spectra Using Density-Functional Force Fields. *J. Phys. Chem.* **1994,** *98,* 11623–11627.
45. Møller, C.; Plesset, M. S. Note on an Approximation Treatment for Many-Electron Systems. *Phys. Rev.* **1934,** *46,* 618–622.
46. Frisch, M. J.; Pople, J. A.; Binkley, J. S. Self-Consistent Molecular-Orbital Methods. 25. Supplementary Functions for Gaussian-Based Sets. *J. Chem. Phys.* **1984,** *80,* 3265–3269.
47. Schlegel, H. B. Potential-Energy Curves Using Unrestricted Moller-Plesset Perturbation Theory with Spin Annihilation. *J. Chem. Phys.* **1986,** *84,* 4530–4534.
48. Mayer, I. The Spin-Projected Extended Hartree-Fock Method. *Adv. Quantum Chem.* **1980,** *12,* 189–262.
49. Curtiss, L. A.; Raghavachari, K.; Pople, J. A. Gaussian-2 Theory Using Reduced Moller-Plesset Orders. *J. Chem. Phys.* **1993,** *98,* 1293–1298.
50. Curtiss, L. A.; Raghavachari, K.; Trucks, G. W.; Pople, J. A. Gaussian-2 Theory for Moelcular Energies of First-Row and Second-Row Compounds. *J. Chem. Phys.* **1991,** *94,* 7221–7230.
51. Pople, J. A.; Head-Gordon, M.; Raghavachari, K. Quadratic Configuration-Interaction. A General Technique for Determining Electron Correlation Energies. *J. Chem. Phys.* **1987,** *87,* 5968–5975.
52. Cizek, J.; Paldus, J.; Sroubkova, L. Cluster Expansion Analysis for Delocalized Systems. *Int. J. Quantum Chem.* **1969,** *3,* 149–167.
53. Purvis, G. D.; Bartlett, R. J. A Full Coupled-Cluster Singles and Doubles Mode. The Inclusion of Disconnected Triples. *J. Chem. Phys.* **1982,** *76,* 1910–1918.
54. Dunning, T. H., Jr. Gaussian Basis Sets for Use in Correlated Molecular Calculations. 1. The Atoms Boron Through Neon and Hydrogen. *J. Chem. Phys.* **1989,** *90,* 1007–1023.
55. Tureček, F. Proton Affinity of Dimethyl Sulfoxide and Relative Stabilities of C_2H_6OS molecules and $C_2H_7OS^+$ ions. *J. Phys. Chem. A* **1998,** *102,* 4703–4713.
56. Tureček, F. Wolken J. K. Dissociation Energies and Kinetics of Aminopyrimidinium Radicals by ab initio and Density Functional Theory. *J. Phys. Chem. A* **1999,** *103,* 1905–1912.
57. Tureček, F.; Carpenter, F. H. Glycine Radicals in the Gas Phase. *J. Chem. Soc. Perkin Trans. 2* **1999**, *11,* 2315–2323.
58. Tureček, F.; Polášek, M.; Frank, A. J.; Sadílek, M. Transient Hydrogen Atom Adducts to Disulfides. Formation and Energetics. *J. Am. Chem. Soc.* **2000,** *122,* 2361–2370.
59. Zhu, L.; Hase, W. L. *Quantum Chemistry Program Exchange*; Indiana University: Bloomington, 1994; Program No. QCPE 644.
60. Frank, A. J.; Sadílek, M.; Ferrier, J. G.; Tureček, F. Sulfur Oxyacids and Radicals in the Gas Phase. A Variable-Time Neutralization-Photoexcitation-Reionization Mass Spectrometric and ab initio/RRKM Study. *J. Am. Chem. Soc.* **1997,** *119,* 12343.
61. Foresman, J. B.; Head-Gordon, M.; Pople, J. A.; Frisch, M. J. Towards a Systematic Molecular-Orbital Theory for Excited States. *J. Phys. Chem.* **1992,** *96,* 135–149.
62. Stratmann, R. E.; Scuseria, G. E.; Frisch, M. J. An Efficient Implementation of Time-Dependent Density-Functional Theory for the Calculation of Excitation Energies of Large Molecules. *J. Chem. Phys.* **1998,** *109,* 8218–8224.
63. NIST Standard Reference Database No. 69. February 2000 release. http//:webbook.nist.gov.
64. Holmes, J. L.; Osborne, A. D. A Simple Method for the Evaluation of the Average Kinetic Energy Released in a Fragmentation Producing a Gaussian-Type Metastable Peak. *Org. Mass Spectrom.* **1981,** *16,* 236.

65. Pedley, J. B.; Naylor, R. D.; Kirby, S. P. *Thermodynamic Data of Organic Compounds; 2nd ed.* Chapman and Hall: London, 1986.
66. Bartmess, J. E.; Scott, J. A.; McIver, R. T., Jr. Scale of Acidities in the Gas Phase from Methanol to Phenol. *J. Am. Chem. Soc.* **1979,** *101,* 6046–6056.
67. Dang, T. T.; Motell, E. L.; Travers, M. J.; Clifford, E. P.; Ellison, G. B.; Depuy, C. H.; Bierbaum, V. M. Experimental and Computational Studies of Deuterated Ethanols. Gas-Phase Acidities, Electron Affinities, and Bond-Dissociation Energies. *Int. J. Mass Spectrom. Ion Proc.* **1993,** *123,* 171–185.
68. Ramond, T. M.; Davico, G. E.; Schwartz, R. L.; Lineberger, W. C. Vibronic Structure of Alkoxy Radicals via Photoelectron Spectroscopy. *J. Chem. Phys.* **2000,** *112,* 1158–1169.
69. Xu, K. S.; Zhang, J. S. Photodissociation of the Vinyl Radical (C_2H_3) via the First Excited State: The $C_2H_2([X]^1\Sigma^+_g)$ + H channel. *J. Chem. Phys.* **1999,** *111,* 3783–3786.
70. Nguyen, V. Q.; Tureček, F. Energy Effects in Collisional Neutralization with Organic Molecules. *J. Mass Spectrom.* **1996,** *31,* 843–854.
71. Leeck, D. T.; Kenttamaa, H. I. Heat of Formation of the Radical-Cation of Dimethyl Disulfide. *Org. Mass Spectrom.* **1994,** *29,* 106–107.
72. Kimura, K.; Osafune, K. Photoelectron Spectroscopic Study of Skew Compounds. III. N,N'-Dimethylhydrazine, Dimethyl Peroxide, and Dimethyl Disulfide. *Bull. Chem. Soc. Jpn.* **1975,** *48,* 2421–2427.
73. Nguyen, V. Q.; Sadílek, M.; Frank, A. J.; Ferrier, J. G.; Tureček, F. Metastable States of Dimethylammonium Radical. *J. Phys. Chem. A* **1997,** *101,* 3789–3799.
74. (a) Sadílek, M.; Tureček, F. Laser Photolysis of $ND_4^{\cdot}$ and Trimethylamine Formed by Collisional Neutralization of Their Cations in the Gas Phase. *Chem. Phys. Lett* **1996,** *263,* 203–207. (b) Frank, A. J. ; Sadílek, M.; Ferrier, J. G.; Tureček, F. Sulfur Oxyacids and Radicals in the Gas Phase. A Variable-Time Neutralization-Photoexicitation-Reionization Mass Spectrometric and ab initio/RRKM Study. *J. Am. Chem. Soc* **1997,** *119,* 12343–12353. (c) Frank, A. J.; Tureček, F. Methylsulfonyl and Methoxysulfinyl Radicals and Cations in the Gas Phase. A Variable-Time and Photoexcitation Neutralization-Reionization and ab initio/RRKM Study. *J. Phys. Chem. A* **1999,** *103,* 5348–5361. (d) Polášek, M.; Tureček, F. Direct Observation of Hydrogen Atom Adducts to Nitromethane and Methyl Nitrite. A Variable-Time Neutralization-Reionization Mass Spectrometric and ab initio/RRKM Study. *J. Phys. Chem. A* **1999,** *103,* 9241–9251. (e) Polášek, M.; Tureček, F. Nitromethyl Radical, Cation, and Anion. A Neutralization and Electron Photodetachment-Reionization Mass Spectrometric and ab initio Computational Study of $[C,H_2,N,O_2]$ Isomers. *J. Phys. Chem. A* **2001,** *105,* 1371–1382.
75. (a) Jortner, J.; Rice, S. A.; Hochstrasser, R. M. Radiationless Transitions in Photochemistry. *Adv. Photochem.* **1969,** *7,* 149–309. (b) Fischer, G. *Vibronic Coupling*. Academic Press: London, 1984, 29–46.